Astronomy & Astrophysics

Identification of different types of kink modes in coronal loops: principles and application to TRACE results

T. J. Wang[1,2], S. K. Solanki[3], and M. Selwa[1]

[1] Department of Physics, Catholic University of America and NASA Goddard Space Flight Center, Code 671, Greenbelt, MD 20771, USA
e-mail: wangtj@helio.gsfc.nasa.gov
[2] Department of Physics, Montana State University, Bozeman, MT 59717-3840, USA
[3] Max-Planck-Institut für Sonnensystemforschung, 37191 Katlenburg-Lindau, Germany

ABSTRACT

We explore the possible observational signatures of different types of kink modes (horizontal and vertical oscillations in their fundamental mode and second harmonic) that may arise in coronal loops, with the aim of determining how well the individual modes can be uniquely identified from time series of images. A simple, purely geometrical model is constructed to describe the different types of kink-mode oscillations. These are then "observed" from a given direction. In particular, we employ the 3D geometrical parameters of 14 TRACE loops of transverse oscillations to try to identify the correct observed wave mode. We find that for many combinations of viewing and loop geometry it is not straightforward to distinguish between at least two types of kink modes just using time series of images. We also considered Doppler signatures and find that these can help obtain unique identifications of the oscillation modes when employed in combination with imaging. We then compare the modeled spatial signatures with the observations of 14 TRACE loops. We find that out of three oscillations previously identified as fundamental horizontal mode oscillations, two cases appear to be fundamental vertical mode oscillations (but possibly combined with the fundamental horizontal mode), and one case appears to be a combination of the fundamental vertical and horizontal modes, while in three cases it is not possible to clearly distinguish between the fundamental mode and the second-harmonic of the horizontal oscillation. In five other cases it is not possible to clearly distinguish between a fundamental horizontal mode and the second-harmonic of a vertical mode.

Key words. Sun: corona – Sun: flares – Sun: oscillations – Sun: UV radiation

1. Introduction

The solar corona is characterized by highly dynamic loop-like structures believed to outline magnetic field lines. Various types of coronal loop oscillations have been observed for decades in radio, visible, EUV, and X-rays (see, e.g., reviews by Nakariakov 2003; Nakariakov & Verwichte 2005; Aschwanden 2004; Wang 2004, 2005). Recently, temporally and spatially resolved transverse and longitudinal oscillations have been detected in coronal loops in the high-resolution observations by the Transition Region And Coronal Explorer (TRACE) and the Solar and Heliospheric Observatory (SOHO). Compressible longitudinal waves in cool (~1 MK) loops were first detected by the EUV Imaging Telescope (EIT) on board SOHO (Berghmans & Clette 1999), which were confirmed by TRACE observations (e.g. De Moortel et al. 2000, 2002a,b), and identified as propagating slow magnetoacoustic waves (Nakariakov et al. 2000). Global kink-mode oscillations were first found in cool (~1 MK) coronal loops from TRACE EUV imaging observations (Aschwanden et al. 1999, 2002; Nakariakov et al. 1999). They were seen as spatial displacements with periods of 3−5 min and were apparently excited by flares or erupting filaments (Aschwanden et al. 2002; Schrijver et al. 2002). Later, strongly damped standing slow-mode waves were discovered with the Solar Ultraviolet Measurement of Emitted Radiation (SUMER) spectrometer

on-board SOHO by virtue of their Doppler signatures in the flare lines Fe XIX and Fe XXI (e.g. Wang et al. 2002, 2003a,b; Ofman & Wang 2002). These oscillations are usually set up immediately following a pulse of hot plasma flowing from one of the loop footpoints, associated with small flares or even microflares (Wang et al. 2005, 2006). Extensive studies on coronal loop oscillations in recent years have made *MHD coronal seismology* a practical, new tool for the determination of previously poorly known parameters of the coronal structure (see, e.g., Roberts et al. 1984; Roberts & Nakariakov 2003; Nakariakov & Verwichte 2005, for reviews). For example, the measured oscillation period has been applied to determine the mean magnetic field strength of coronal loops in case of either kink mode (Nakariakov & Ofman 2001; Verwichte et al. 2004) or slow mode oscillations (Wang et al. 2007).

Wang & Solanki (2004) first suggested that the longitudinal curvature of loops may lead to two types of kink modes (i.e., horizontal and vertical modes) in a coronal loop based on observations. The motion is termed a *horizontal* mode if the loop rocks perpendicularly to the loop plane. If the oscillation is polarized in the loop plane and manifests expanding and shrinking motions, we refer to it as a *vertical* mode. The horizontal kink mode oscillation for an individual loop has been numerically studied by Miyagoshi et al. (2004) with a 3D MHD model. They set an initial horizontal velocity field near the loop top

as a perturbation to induce the oscillation. The vertical mode oscillation can be excited either by a pressure pulse below the loop apex (e.g. Selwa et al. 2005, 2006, 2007) or by a velocity driver in one of the footpoints (e.g. Brady & Arber 2005; Brady et al. 2006; Verwichte et al. 2006a,b) as simulated in a 2D arcade model. Very recently, McLaughlin & Ofman (2008) performed a 3D nonlinear MHD simulation of wave activity in active regions in which individual loop density structure is included. They found that the impact of the fast wave impulsively excites both horizontal and vertical loop oscillations. Van Doorsselaere et al. (2004) first studied the eigenmodes of a curved loop and showed that curvature only slightly affects the damping times of the observed kink oscillations in comparison with a straight tube. By numerically solving the eigenvalue problem of a similar model, Terradas et al. (2006) found that curvature and density structuring introduce preferential directions of oscillation showing the existence of two kink eigenmodes with horizontal and vertical polarizations, but their frequencies and damping rates are very similar. Their calculation supports the initial notion of Wang & Solanki (2004).

In several examples, the second harmonic was found together with the fundamental mode via time series analysis (Verwichte et al. 2004; Van Doorsselaere et al. 2007). The first spatially resolved example of the second harmonic of transverse loop oscillations was recently identified by De Moortel & Brady (2007). Díaz et al. (2006) and Díaz (2006) analytically studied the vertical kink mode and its second harmonic (they termed it the *swaying* kink mode). Observations of multiple periodicities in kink loop oscillations (e.g., Verwichte et al. 2004) have been used to extract information on the internal longitudinal structuring of coronal loops by Andries et al. (2005), McEwan et al. (2006) and has been demonstrated to have high potential value for coronal seismology. In addition, Terradas et al. (2007) theoretically studied the excitation of the eigenmodes of coronal loops due to an initial disturbance. Their results suggest that longitudinal harmonics of kink modes are in principle more easily excited than azimuthal harmonics (fluting modes).

Therefore, differentiating between various types of kink modes and their higher harmonics in observations will improve the applications of coronal seismology in precisely determining the unknown physical parameters of the coronal plasma. Aschwanden et al. (2002) identified oscillations in 26 coronal loops as kink modes. They did not distinguish between the different types of modes. Wang & Solanki (2004) have for the first time identified the vertical kink mode oscillation of a TRACE loop above the limb based on its spatial signature, which is distinct from the horizontal mode. Our aim here is to explore observational signatures of different types of kink-mode oscillations based on the loop geometries measured by Aschwanden et al. (2002) and check if each observed oscillation can be identified with a given type of kink mode based on these signatures.

In Sect. 2, we describe the methods which are used to model the horizontal and vertical kink modes. In Sect. 3, we discuss their similarities and differences in signatures of the spatial pattern and Doppler shift. In Sect. 4, we discuss the simultaneous presence of multiple (harmonics) modes. Conclusions are summarized in Sect. 5.

2. Modeling of different types of kink mode oscillations

In principle we need to solve the three-dimensional MHD wave equations to first obtain the eigenfunction and then use it to analyze the motion of the eigenmodes of coronal loops (e.g., Van Doorsselaere et al. 2004; Terradas et al. 2006). Since the aim of this paper is to provide a simple guide to interpret observations, we model the loop oscillations based on simple geometric considerations. The loops are assumed to be symmetric circular arches lying in a plane, but it is cautioned that in general real loops do not satisfy this condition. We set up a Cartesian coordinate system (x, y, z) with the origin at the midpoint between the two footpoints of the loop. The x-axis is along the loop baseline, and the z-axis is directed towards the apex of the loop. The position of a point along the loop is first transformed from the Cartesian system into the spherical polar system, with the coordinates (R, ϕ, ψ), where the y-axis is taken to be the axis of rotation. R, ϕ and ψ are the radius, latitude and longitude, respectively.

We model horizontal oscillations by modulating the latitude ϕ in the form,

$$\phi(\psi, t) = \phi_m \cos \psi \sin \omega_1 t \quad \text{(for fundamental mode),} \tag{1}$$

or

$$\phi(\psi, t) = \phi_m \sin 2\psi \sin \omega_2 t \quad \text{(for second harmonic),} \tag{2}$$

where ψ runs between $-\pi/2$ and $\pi/2$ for a point along the loop between its two footpoints, ϕ_m is a small constant, representing the maximum amplitude, ω_1 and ω_2 are the oscillation frequencies for the fundamental mode and the second harmonic. The equilibrium position of the loop is given when $\phi_m = 0$. Figures 1a and b illustrate the fundamental mode and second harmonic horizontal oscillations of a semi-circular loop, modeled by taking $R(\psi, t)$ as the form given by Eqs. (1) and (2), respectively.

We model vertical oscillations by modulating the radius R,

$$R(\psi, t) = R(\psi)(1 + A_m \cos \psi \sin \omega_1 t) \quad \text{(for fundamental mode),} \tag{3}$$

or

$$R(\psi, t) = R(\psi)(1 + A_m \sin 2\psi \sin \omega_2 t) \quad \text{(for second harmonic),} \tag{4}$$

where A_m is a small constant representing the relative maximum displacement amplitude, ω_1, ω_2, and ψ have the same definitions as in Eqs. (1) and (2). Figures 1c and d illustrate the fundamental mode and second harmonic vertical oscillations of a semi-circular loop, modeled by taking $R(\psi, t)$ as the form given by Eqs. (3) and (4), respectively.

Díaz et al. (2006) analytically studied oscillation modes of a 2D semi-circular magnetic arcade. They named the solution of the wave equation with an azimuthal wavenumber of $m = 1$ the vertical mode and the solution with $m = 2$ as the swaying mode. The fundamental vertical and the swaying modes correspond to the fundamental and second harmonic kink modes, respectively, in the straight flux slab or cylindrical tube (Edwin & Roberts 1982, 1983).

3. The modeled signatures for 14 TRACE loops

3.1. Observations

Transverse oscillations of 26 coronal loops observed by TRACE in the 171 Å and 195 Å wavelength bands have been analyzed by Aschwanden et al. (2002). They interpreted these oscillations in terms of fast kink modes, but did not consider their possible classification. Here we select 14 of these loops (see Table 1) to model the horizontal and vertical oscillations in their
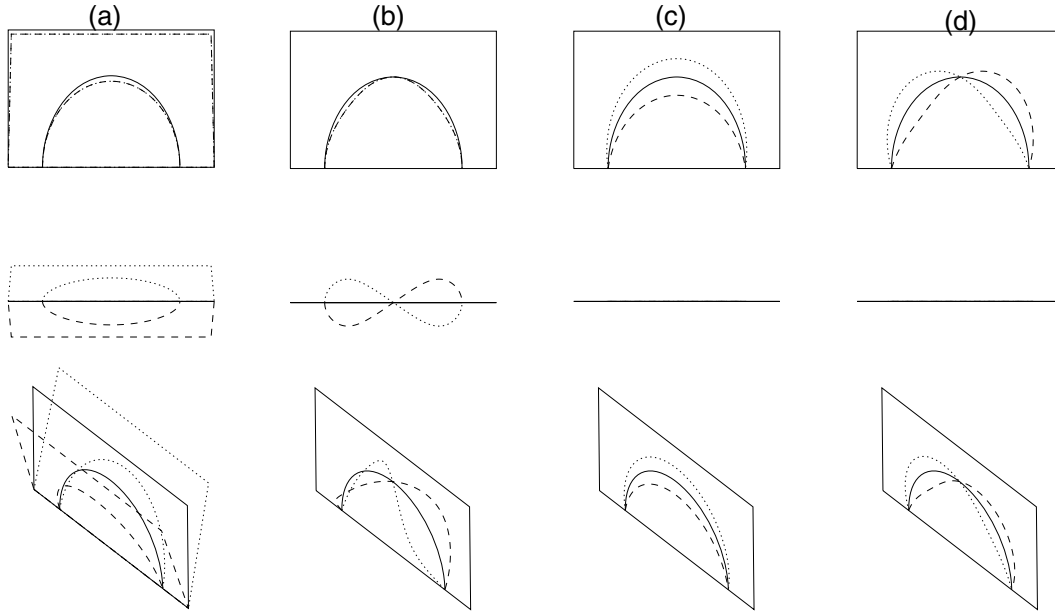
Fig. 1. A sketch of the horizontal and vertical oscillations and their second harmonics. **a)** The fundamental horizontal mode, **b)** the second harmonic horizontal mode, **c)** the fundamental vertical mode, and **d)** the second harmonic vertical mode. *The top, middle and bottom rows* correspond to views from the side, *top and top-left*, respectively.

Table 1. Geometrical parameters of the analyzed TRACE oscillating loops[a], which are taken from Aschwanden et al. (2002).

Loop No	$l_0 - l_c$ (deg)	$b_0 - b_c$ (deg)	α (deg)	θ_0 (deg)	h_0 Mm	r (Mm)	γ (deg)	Aschwanden et al. (2002)	Geom. Category	Likely Mode[b]	Multiple Modes
1	−15.6	−27.6	87	7	9	47	20	1a, Fig. 3	III	1H	
2	−19.6	−24.5	12	−44	11	57	54	1f, Fig. 4	I	1H	
3	82.3	−27.7	152	−12	38	99	25	3a, Fig. 5	II	1H or 2V	
4	26.0	−27.3	7	−14	12	74	40	4a, Fig. 6	I	1H or 2H	
5	−22.9	−21.3	47	2	0	53	7	5c, Fig. 7	III	1H	
6	70.7	16.4	158	22	28	43	30	7a, Fig. 8	II	1H, 2H or 2V	
7	25.6	−8.6	143	53	−8	30	54	8a, Fig. 9	I	1H or 2H	
8	72.6	−3.8	157	20	67	77	25	10a, Fig. 10	II	1H or 2V	
9	78.9	−6.3	25	−30	43	47	26	11a, Fig. 11	II		1H+1V
10	49.2	−20.2	150	49	−71	120	37	12b, Fig. 12	I	1H or 2H	
11	75.2	−21.8	10	−22	42	48	19	14a, Fig. 13	II	1H, 2H or 2V	
12	−4.7	−18.8	99	63	−10	65	63	15a, Fig. 14	I	1V[c]	1H+1V
13	22.7	−18.3	177	−39	−11	68	49	16a, Fig. 15	I	1V	1H+1V
14	−48.7	−28.0	1	−41	19	33	38	17a, Fig. 16	II	1H or 2V	

[a] $l_0 - l_c$ and $b_0 - b_c$ are the heliographic longitude and latitude relative to Sun center for the midpoint of the loop footpoint baseline. α is the azimuth angle of the loop baseline to the east-west direction. θ_0 is the inclination angle of the loop plane to the vertical. h_0 is the height of the center of the circle describing the loop in the loop plane. r is the radius of the circular loop. γ is the inclination angle of the loop plane to the line-of-sight direction. The column named "Aschwanden et al. (2002)" lists the case and corresponding figure numbers in that paper. The last third column lists the category of viewing geometry for loops. The last two columns list the type of likely single and multiple kink modes identified by comparing the observed signature with our geometrical model.
[b] 1H and 2H indicate the fundamental and the second-harmonic horizontal oscillations, respectively, 1V and 2V the fundamental and the second-harmonic vertical oscillations. 1H+1V indicates a combination of the fundamental horizontal and vertical modes.
[c] This case was recently re-examined and identified as the second harmonic horizontal mode by De Moortel & Brady (2007), based on the presence of an apparent node (see the text).

fundamental mode and second harmonic in order to discuss if the types of these kink oscillations can be uniquely identified based on their signatures in TRACE movies. We chose these examples because they were illustrated by Aschwanden et al. (2002) in their paper and we can easily compare our modeled results with their figures. As we shall show in Sect. 3.2, imaging alone often does not allow a unique identification. We therefore also consider if the spectroscopic signature of these modes is helpful to resolve remaining ambiguities (Sect. 3.3). We employ the geometrical parameters of the loops as measured by

Aschwanden et al. (2002). Figure 2 shows the orientations and positions of the sampled loops on the solar disk at the time of the observed oscillation. The loops' geometrical parameters are listed in Table 1.

3.2. Spatial features

For the 14 loops, we model the horizontal oscillation with an amplitude of $\phi_m = 5°$ (or 0.087 arc deg) and model the
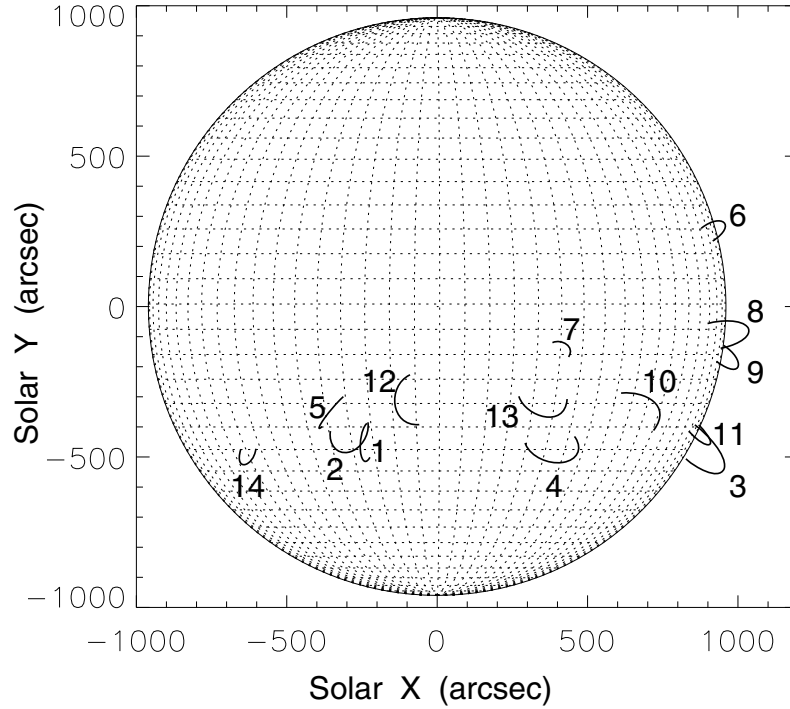
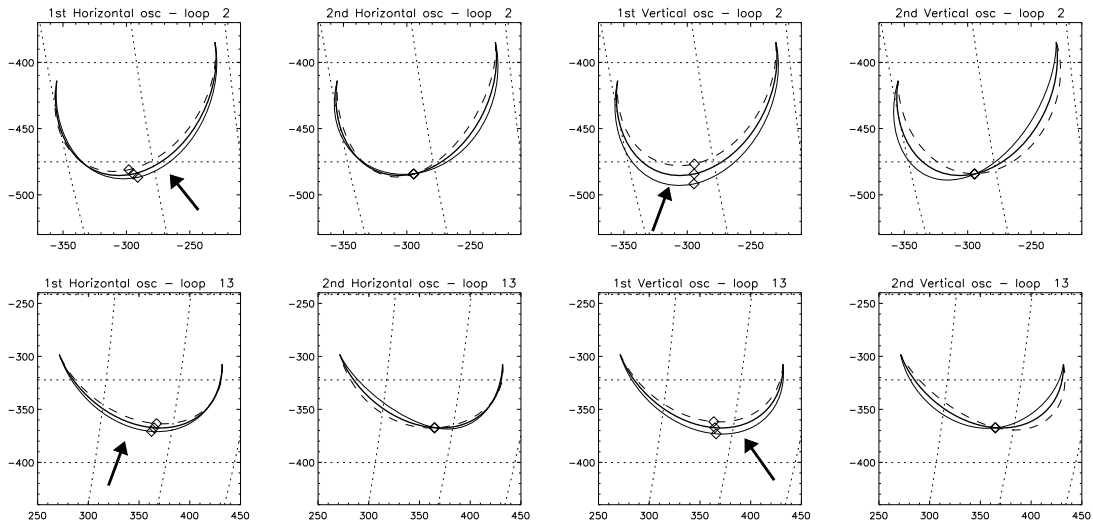**Fig. 2.** Positions of the 14 studied oscillating TRACE loops on the solar disk.

Fig. 3. Comparison between the fundamental mode (*left*) and the second harmonic (*middle left*) of the horizontal oscillation as well as the fundamental mode (*middle right*) and the second harmonic (*right*) of the vertical oscillation for loops with the first category of geometries (loop 2: *top row*, loop 13: *bottom row*). The thick solid lines represent the equilibrium position of the oscillating loop and the thin solid and dashed lines represent the two extrema at opposite phases of the oscillation. The apex position of the loop at each snapshot is indicated by a *diamond*. Arrows indicate the location of maximum displacement due to the horizontal and vertical fundamental oscillation.

vertical oscillation with a relative amplitude of $A_m = 0.087$ (see Sect. 2). Note that we set the same maximum relative amplitudes for the horizontal and vertical oscillations in order to make reasonable comparisons. Based on the similarity and difference in the projected signatures of the four types of kink modes, the 14 loops can be divided into three categories. Some typical cases are shown in Figs. 3–5 and the main characteristics are summarized in Table 2.

– *Category I (Loops 2, 4, 7, 10, 12 and 13)*:
Loops in this category are located close to disk center and their loop planes have a large inclination angle (γ) to the line-of-sight

direction. The values of γ are in the range $37°-63°$ (Table 1). Figure 3 shows two typical examples of such loops. For each of these the observational signature of all four kink modes is illustrated. At first sight the horizontal oscillations have a similar appearance to the vertical oscillations. In the case of the fundamental mode they both exhibit an evident displacement around the loop top in the projected plane (irrespective of whether it is the horizontal or the vertical fundamental mode), while in the case of the second harmonic they show a node at the loop top and maximum displacements at the legs. However, if we scrutinize the position of the point on the loop with the maximum
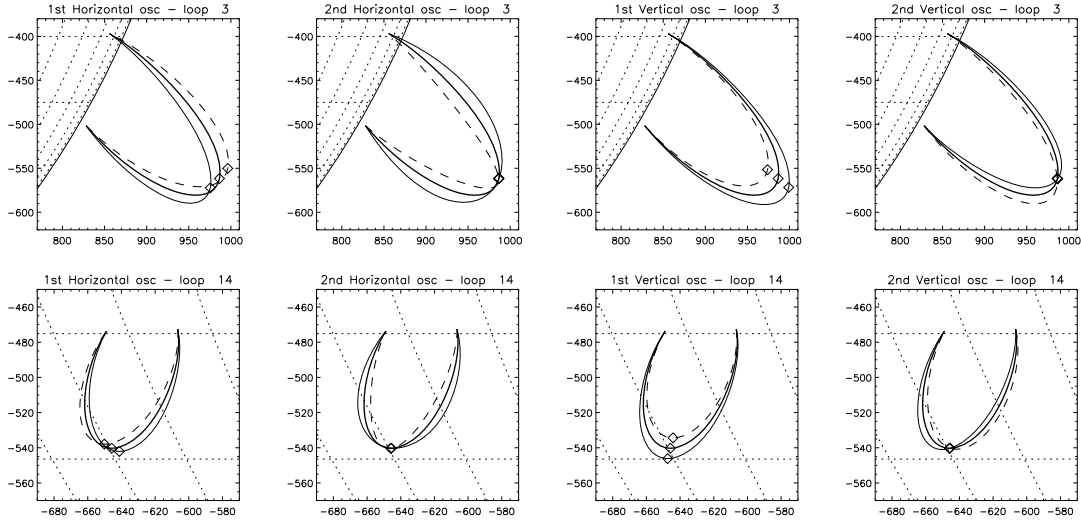
Fig. 4. Same as Fig. 3 but for loops with geometries belonging to the second category (loop 3 on *top* and loop 14 at the *bottom*).
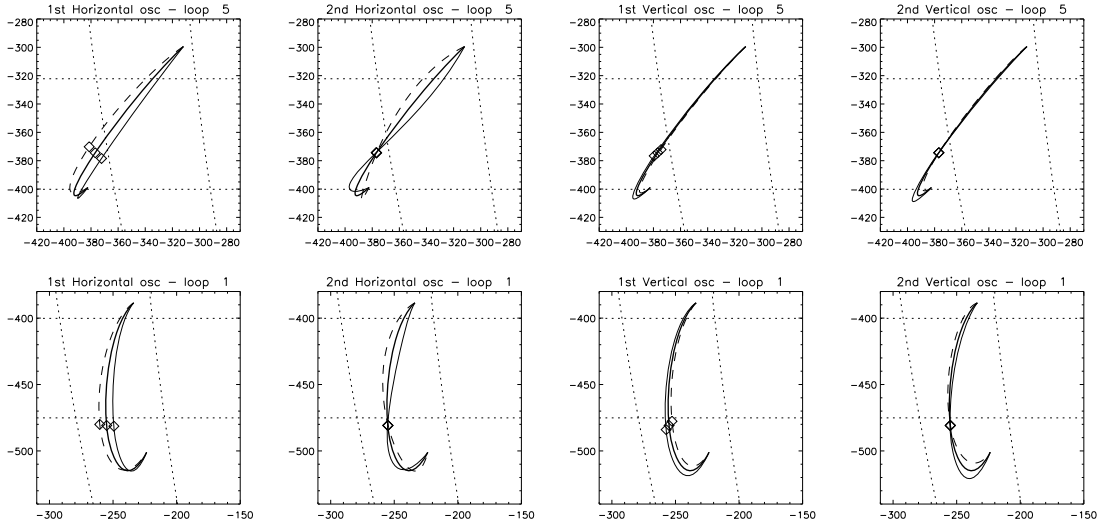

Fig. 5. Same as Fig. 3 but for loops with geometries belonging to the third category: loop 5 in the top row and loop 1 in the bottom row.

projected displacement (indicated by arrows in the first and third column panels of Fig. 3) for the fundamental mode, we find that this point is located on different sides of the loop apex for the horizontal and vertical oscillations (e.g., to the right of the apex of loop 2 for the horizontal mode and to the left for the vertical mode; see arrows in the top first and third panels of Fig. 3). Therefore, we may identify the type of the observed kink oscillations according to the measured position of the most evident displacements. The locations of the most pronounced oscillation for the studied cases have been marked in Figs. 3–16 of Aschwanden et al. (2002). Thus, the observation of transverse oscillations of loop 2 is better explained by the fundamental horizontal mode. For loops 12 (not shown) and 13 (bottom panels of Fig. 3), the location of the most pronounced oscillation from Aschwanden et al. (2002) supports them as the fundamental vertical mode. Note that the case of loop 12 was re-examined by De Moortel & Brady (2007) recently, who identified the oscillation as the second harmonic horizontal mode based on the signature of an apparent node, whereas Aschwanden et al. (2002) measured the oscillation for the top half of the loop by considering the apparent node to be a footpoint, and interpreted

it as the fundamental kink mode. Since the measured oscillation period is peculiar long and better matches the fundamental mode, the interpretation by the second harmonic remains debated.

For the second harmonic, the displacements are evident in only one leg for the horizontal oscillation while they are evident in both legs for the vertical oscillation. The observations of loops 4, 7 and 10 all show oscillations only in one leg, so that they are consistent with the signature of the second harmonic horizontal mode. However, we notice that the fundamental horizontal oscillations also shows an evident displacement mainly in one loop leg, so that we cannot clearly distinguish between these two modes, even when we take into account measurements of their periods. For example, Aschwanden et al. (2002) measured an oscillation period of 136 s and a loop length of 113 Mm for loop 10, yielding an estimate of the phase speed of 830 km s^{-1} for the second harmonic which is in the range of acceptable values.

– *Category II (Loops 3, 6, 8, 9, 11 and 14)*:
Most of the loops in this category are located at the limb, except for loop 14, which is located relatively near the limb. The

two typical examples shown in Fig. 4 reveal that the fundamental horizontal and the second-harmonic vertical oscillations look similar. Both exhibit a cross-over between maxima of the displacement near the loop top. The fundamental vertical oscillation is distinctly different, exhibiting a lateral displacement with the maximum amplitude close to the loop top. Based on these signatures, Wang & Solanki (2004) identified the fundamental vertical kink oscillations of a limb loop in the TRACE 195 Å band. The second-harmonic horizontal oscillation may also be easily distinguished from other types of oscillations. It shows evident displacements at both legs, so that the loop alternates between thin and fat shapes. Aschwanden et al. (2002) showed that the oscillations in all 6 loops in this category are most evident in the loop legs, which is consistent with the signature of the horizontal oscillation or the second-harmonic vertical oscillation. However, the difference images shown in their paper did not clearly reveal cross-over as expected for the fundamental horizontal or the second harmonic vertical mode. Neither did it clearly indicate the change in loop shape expected for the second harmonic horizontal mode. This may be because the two images they used were not taken at the times when the loop is located at the maximum and minimum positions of the oscillations, respectively. The other reason could lie in the fact that in most cases the oscillatory motion of the loop is superimposed on a trend motion (a systematic motion) of the entire loop. Therefore, the expected signatures may be difficult to see. However, the second-harmonic horizontal oscillation should be distinguishable from the other two similar modes, i.e. the fundamental horizontal and the second-harmonic vertical modes, by analyzing the phase relationship of the oscillations at the two loop legs. For the former the displacements are in anti-phase while for the latter the displacements are in phase.

Due to the reasons mentioned above, we re-examined the TRACE data for the 6 loops in this category. The difference image plotted in Fig. 10a shows that loop 9 has an initial displacement most prominent at the loop top, which is consistent with the vertical motion, while the displacements in the following period seem to agree with the combination of the fundamental horizontal and vertical oscillations (see Sect. 4). For loops 3, 8 and 14 the second-harmonic horizontal oscillation can be excluded because their two legs indicate the in-phase motions. For loops 6 and 11 only one of their legs is visible, so that it is only possible to rule out the fundamental vertical mode. The identified possible modes for the 6 loops are listed in Table 1. We shall show in Sect. 3.3 that the Doppler shift observations may help distinguish the fundamental horizontal from the second-harmonic vertical modes, which exhibit very similar spatial signatures.

– Category III (Loops 1 and 5):
Those loops are located on the solar disk with the loop plane inclined only slightly relative to the line of sight. Figure 5 shows two such cases. In this category the fundamental and second-harmonic vertical oscillations show a similar signature in the sense that the oscillation is evident only in a small part, near one end, of the projected loop. It is easily possible to miss such a weak oscillation signature in observations. The horizontal oscillation instead shows clear horizontal displacements over a large part of the loop. Its second harmonic can be easily identified based on a node at the loop apex, for which the displacements on both sides oscillate in anti-phase. Based on the observed signature shown by Aschwanden et al. (2002) we identify the transverse oscillations of loops 1 and 5 as the fundamental horizontal kink mode.

3.3. Doppler features

Spectroscopic observations provide additional information (e.g., Doppler shifts) that may help distinguish between various types of kink modes. Observations of the kink-mode loop oscillations with TRACE thin filters have indicated that the loops did not experience significant heating or cooling during the oscillations, because they were usually seen to exist before and after the events (Schrijver et al. 2002; Aschwanden et al. 2002). Thus, it should be possible to select certain coronal lines with a suitable formation temperature to detect Doppler shift signatures of kink modes in coronal loops and hopefully to distinguish between the different possible modes of oscillation. Here we calculate for four types of kink modes the distribution of Doppler velocity along the loop for a snapshot corresponding to the time of the loop's passage through its equilibrium position. At that time the perturbed velocity of the loop reaches its maximum. The calculated LOS Doppler velocity distributions for an example taken from each of the three categories of loops are shown in Fig. 6. Positive velocity represents redshifts. For comparison purposes, the maximum amplitude of the absolute value of velocities along the loop has been normalized to $100 \ \mathrm{km\,s^{-1}}$ for all modes of oscillation.

We first consider a loop belonging to Category I (e.g., loops 2 and 13 whose Doppler shift is plotted in left panels of Fig. 6). The fundamental horizontal oscillation shows a redshift over the entire loop, with the peak redshift near the middle of the projected loop. The fundamental vertical oscillation shows a redshift over the major part of the loop and a weak blueshift near one end. The second-harmonic horizontal and vertical oscillations both show sinusoidal redshifts over half the loop, but display quite different profiles of Doppler shifts over the other half. Therefore Doppler shift measurements can help distinguish different types of kink modes, especially among those types of oscillations which show a similar spatial signature in this category (fundamental and second harmonic horizontal modes). For that purpose it is sufficient to measure the Doppler shift at two positions in the loop, one in each half.

In Category II (e.g., loops 3 and 14 in Fig. 6, *middle panels*), the fundamental horizontal oscillation shows a similar Doppler signature as in Category I but the peak appears slightly sharper. The Doppler shift signatures of the second-harmonic horizontal and the fundamental vertical oscillations look similar to each other, but different to those of the other modes. The second-harmonic vertical oscillation is characterized by two completely separated (due to a node at the apex) redshift peaks. The fundamental horizontal and the second-harmonic vertical oscillations, which are difficult to distinguish based on the spatial signature (see Sect. 3.2), can be well distinguished based on the Doppler signature. Again, measurements at two locations in the loop, one in the leg, one at the apex, should be sufficient.

Finally, in loops belonging to Category III (loops 1 and 5 in Fig. 6, *right panels*), the horizontal oscillations in both the fundamental and second-harmonic modes have very small amplitudes in Doppler shift due to their motions almost perpendicular to the line-of-sight. Therefore, their Doppler shift oscillations are difficult to be detected. In contrast, the vertical oscillations display large amplitudes in Doppler shift and their fundamental and second-harmonic modes can be easily distinguished based on the Doppler shift profiles along the loop. As we have seen in Sect. 3.2 exactly these two modes are difficult to detect in imaging observations. Therefore, the imaging and spectroscopic detections of the horizontal and vertical oscillations are complementary for this category of loops.
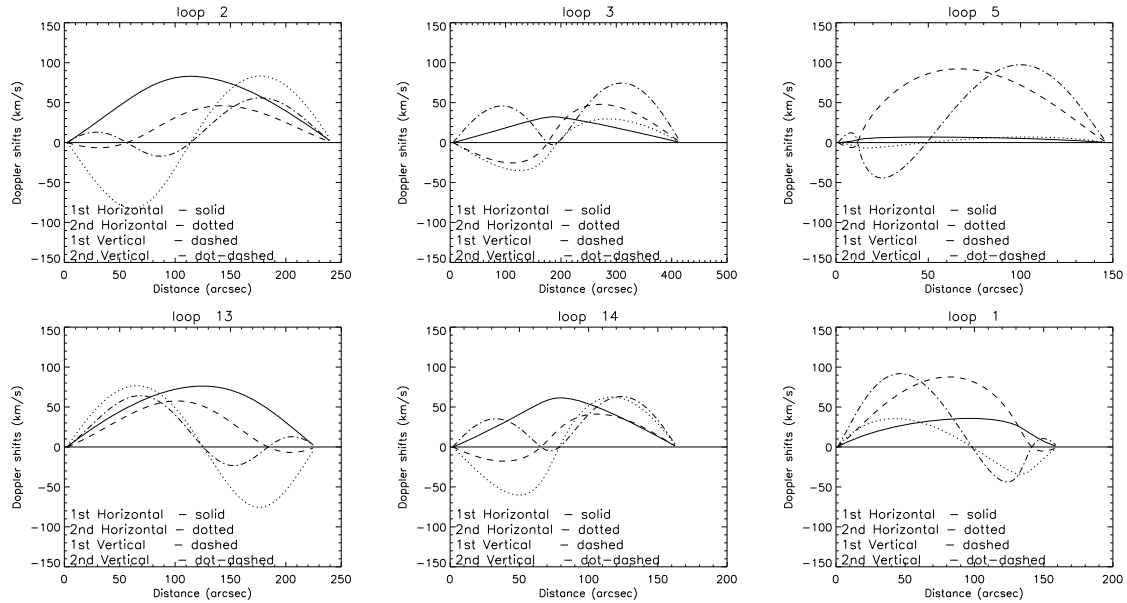
Fig. 6. Comparison of the fundamental horizontal (solid line), the second-harmonic horizontal (dotted line), the fundamental vertical (dashed), and the second-harmonic vertical (dot-dashed) oscillations in the line-of-sight Doppler shift for three categories of loops: I (*left panels*, see Fig. 3), II (*middle panels*, see Fig. 4) and III (*right panels*, see Fig. 5). The maximum amplitudes of the absolute value of velocity along the projected loop for four types of kink modes are normalized to be 100 km s^{-1} in order to facilitate the comparison of Doppler shift profiles. Positive Doppler velocity represents a redshift. On the horizontal axis 0 corresponds to the left footpoint of the oscillating loop.

4. Simultaneous presence of multiple (harmonics) modes

Another reason, besides an inappropriate direction of view, for the failure to identify the mode of oscillation is the possibility of multiple modes being excited in the loop. Such a case would result in more complex features and would make the distinction based on our idea more complicated or sometimes impossible when considering a combination of the fundamental and the second harmonic modes of the same polarization (e.g., for loops 4, 6, 7, 10 and 11) or when considering a combination of the fundamental horizontal and vertical modes (see the following discussion). Two events of the second harmonic of the horizontal kink mode were reported by Verwichte et al. (2004) in a post-flare loop arcade. However, both of them existed together with the fundamental mode. Van Doorsselaere et al. (2007) also found a kink oscillation event showing two wave periods, which are consistent with the periods of the fundamental and the second harmonic modes, respectively. No pure higher harmonic mode has been observed so far. The simultaneous excitation of the fundamental and higher harmonics for the kink modes is also suggested in a theoretical analysis by Terradas et al. (2007).

A good numerical example of simultaneous excitation of both the fundamental and the second harmonic mode (in case of vertical kink oscillations) can be provided by reconsidering the result of simulations described by Selwa et al. (2006). Based on a 2D MHD arcade loop model, Selwa et al. (2006) showed that a pulse launched near one of the footpoints can excite multiple oscillation modes, in particular a swaying-like (possible second-harmonic vertical) mode overlaid on a fundamental vertical mode that results in shifts of the apex. Figure 7 shows the positions of a field line within the oscillating loop at four points in time. We notice a sideways motion of the upper part of the loop. The ratio of the oscillation period of the swaying-like mode to that of the fundamental vertical mode, which is measured to be about 0.75, agrees well with the theoretically predicted value (see Table 1 in Díaz et al. 2006, where the second-harmonic
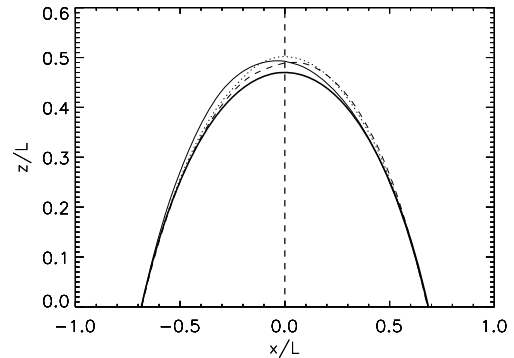

Fig. 7. MHD simulations of swaying-like loop oscillations excited by a hot pulse launched at $(x_0/L, z_0/L) = (-0.42, 0)$ where $L = 100$ Mm (for details see Selwa et al. 2006). The curves indicate the positions of a field line in the oscillating loop at a series of times: $t = 0$ (thick solid line), $t = 200$ s (thin solid line), $t = 300$ s (dotted line), and $t = 375$ s (dashed line).

vertical oscillation is termed the swaying mode). This indicates that the swaying signature seen in the simulation may be caused by the overlaping of the fundamental and the second-harmonic vertical modes. Moreover, Selwa et al. (2006) found that the swaying-like mode dampens less efficiently than the fundamental vertical mode. This feature is consistent with the property of energy leakage as the dominant damping mechanism, i.e., the damping is weaker for higher harmonics (e.g., Verwichte et al. 2006a).

Since the fundamental horizontal and vertical modes are the most probable eigenmodes of the kink oscillation and have very similar periods and damping times (Terradas et al. 2006), it is likely that the two polarizations are excited simultaneously depending on the exciter and how the blast wave interacts with the loops. As a comparison with the single modes, we calculate the spatial and Doppler shift signatures of the combined fundamental horizontal and vertical modes (see Figs. 8 and 9). The
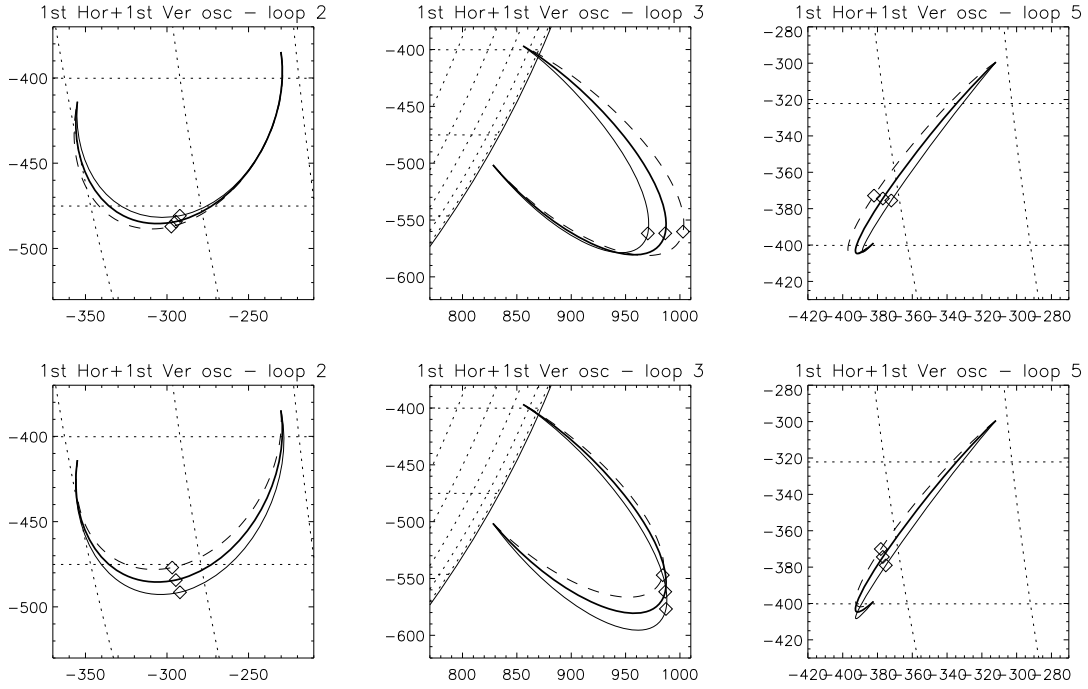
Fig. 8. Spatial signatures of the combined fundamental horizontal and vertical modes for three loops, each observed from a different direction. For the two polarization components the same maximum relative amplitudes are assumed and two phase relations are considered. (*Top panels*) Case A – The dashed line represents the extreme position when the loop is expanding while horizontally moving northward and the thin solid line the extreme at opposite phase. (*Bottom panels*) Case B – The horizontal oscillation component keeps the same phase but the vertical oscillation component has an opposite phase to the above case.
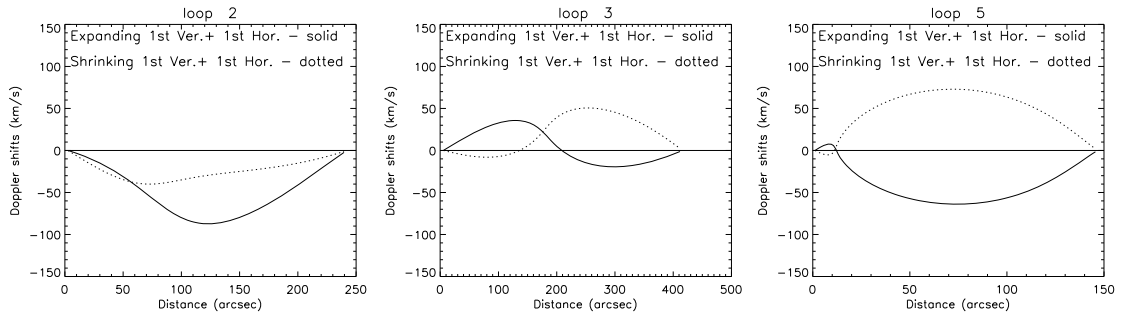

Fig. 9. Doppler shift signatures of the combined fundamental horizontal and vertical modes for the loops plotted in Fig. 8. The solid curve represents the case shown in case A (*the top panels* of Fig. 8), while the dotted curve for case B (*the bottom panels* of Fig. 8).

same relative amplitudes are assumed for the two polarization components, i.e., $A_m = \phi_m = 0.062$ (arc deg), so that the total maximum relative amplitude is about $\sqrt{2}A_m = 0.087$, same as used to model the single modes in Sect. 3. Two cases are considered, in which the vertical oscillation components have the opposite phase while the horizontal oscillation component retains its phase. We refer to the case shown in the upper panels of Fig. 8 as case A, and the case in the bottom panels as case B. The main spatial and Doppler shift characteristics are summarized in Table 2.

The loops belonging to Catogory I show an evident displacement at one leg in the projected plane in case A (e.g., Fig. 8 *top left*), which can be easily distinguished from the four types of kink modes analyzed in Sect. 3.2. Note that the fundamental and second harmonic horizontal modes display an evident displacement at the other leg. However, in case B they exhibit an evident displacement around the loop top (e.g., Fig. 8 *bottom*

left), which looks very similar to that for the fundamental vertical mode. Therefore, we cannot exclude the possibility that the fundamental vertical oscillation which has been identified for loops 12 and 13 is combined with the fundamental horizontal mode in this case. By comparing their Doppler shift signatures (the dotted curve in Fig. 9 *left* and the dashed curve in Fig. 6 *top left*), we find that their peak shifts are located at different sides of the projected loop. Thus the combined fundamental horizontal and vertical modes may be distinguished from the single fundamental vertical mode based on the measurement of the Doppler shift at two positions in the loop, one in each half in case B.

For the loops in Category II, we find that the combined fundamental horizontal and vertical modes can be uniquely identified, because they display an evident displacement off the loop top in both cases (e.g., Fig. 8 *middle*), which are clearly different from the features of the four types of kink modes analyzed in Sect. 3.2. The TRACE difference images reveal that for loop 9 its

Table 2. Comparison of spatial and Doppler shift signatures for four types of single kink mode and the combined fundamental horizontal and vertical modes[a].

Category	Definition	Spatial signatures	Doppler shift signatures	Examples
I	loops located near disk center and loop plane inclined to LOS by 40°–60°	1H, 2H and 1V look similar, while 2V is distinctly different from others. In case A, 1H+1V can be distinguished from the four single modes. In case B, 1H+1V and 1V look similar.	1H ans 2H can be easily distinguished, but 1H and 1V cannot be. 1H+1V and 1V can be distinguished in case B.	Loops 2, 4, 7, 10, 12, 13
II	loops located near the limb	1H and 2V look similar, and they may be distinguished from 2H, while 1V is distinctly different. In both cases 1H+1V can be easily distinguished from the four single modes.	1H and 2V can be easily distinguished. 2H and 1V look similar. 1H+1V may look similar to 2H or 1V.	Loops 3, 6, 8, 9, 11, 14
III	loops located on disk and loop plane nearly parallel to LOS	1V and 2V look similar, and are hard to detect, but can be easily distinguished from 1H and 2H. In both cases 1H+1V looks similar to 1H.	1H and 2H are poorly detectable. 1V and 2V can be easily distinguished. 1H+1V can be easily distinguished from 1H.	Loops 1, 5

[a] 1H and 2H indicate the fundamental and the second-harmonic horizontal oscillations, respectively, 1V and 2V the fundamental and the second-harmonic vertical oscillations. 1H+1V indicates a combination of the fundamental horizontal and vertical modes. The definitions for cases A and B are given in Sect. 4.
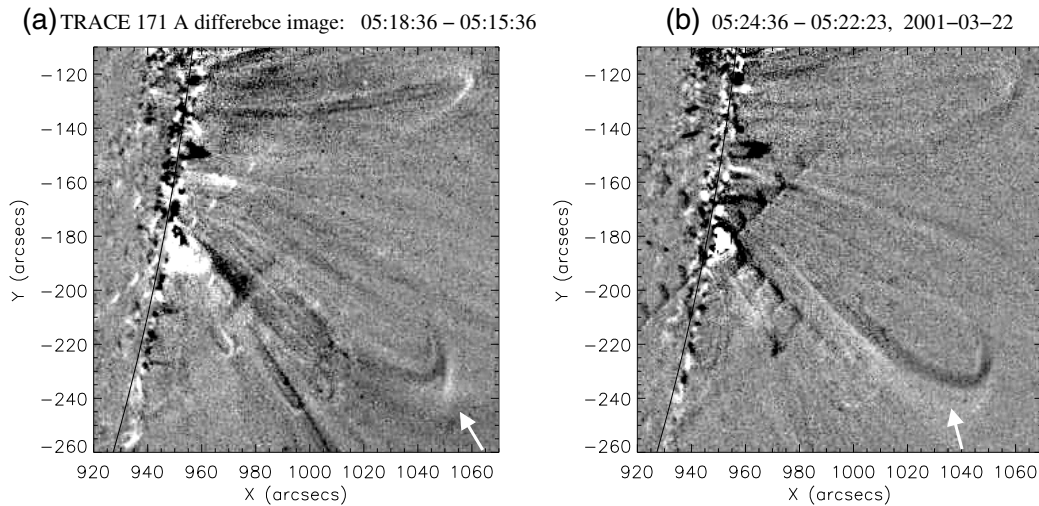
Fig. 10. Transverse oscillation of loop 9 seen in TRACE 171 Å difference images. The dark regions represent the loop seen in the earlier map and the white regions represent the loop in the current map. Evident motions of the loop are indicated by a white arrow.

initial apparent displacement is consistent with vertical motion (Fig. 10a), while the displacements at the following phase consistent with the combined fundamental and vertical oscillations (comparing Figs. 10b with 8 *bottom middle*). It is also possible to distinguish between combined modes with different phase relationships on the basis of the skew direction of their evident displacements.

For the loops in Category III, both cases of the combined fundamental horizontal and vertical modes show the feature of horizontal displacements very similar to the single fundamental horizontal mode, but they can be easily distinguished from the horizontal mode based on the large Doppler shifts along the loop (Fig. 9 *right*).

5. Discussion and conclusion

We have modeled the geometric distortion to a simple circular loop produced by four types of kink modes (fundamental and

second harmonic modes of horizontal and vertical oscillations) and considered if it is possible to distinguish between them for a given observational geometry. We analyzed in detail 14 selected TRACE loops observed to harbor transverse oscillations and found that they can be divided into three categories based on the location of the observer relative to the loop plane (viewing geometry). The apparent similarity and difference between the four types of kink modes in spatial signatures is found to depend strongly on the category. We also examined if the kink modes displaying a similar spatial signature can be distinguished based on their Doppler shift signatures. Our main conclusions regarding the possibility of distinguishing between modes are outlined below (see also Table 2).

(1) For those loops whose loop plane is almost in the line-of-sight direction (i.e. loops in Category III), the fundamental and second-harmonic horizontal kink modes can be easily and uniquely identified based on the signature of evident lateral displacements of the loop. The fundamental and second-harmonic

vertical kink modes show smaller displacements with similar signature in this viewing geometry and are difficult to detect and distinguish. It is also impossible to determine if a fundamental horizontal mode is combined together with a fundamental vertical mode in this case. For those loops located on or near the limb (e.g. Category II loops), the fundamental vertical kink mode as well as its combination with the fundamental horizontal mode are most easy to distinguish from the other types of kink modes. The fundamental horizontal and the second-harmonic vertical modes look similar, displaying a cross-over signature near the loop top. For those loops on the solar disk whose loop plane is inclined at an angle sufficiently different from 0° and 90° to the line-of-sight direction (e.g., the loops in Category I), the second-harmonic vertical mode is most easy to be uniquely identified based on the cross-over signature near the loop top. The fundamental horizontal and vertical oscillations may be distinguished from each other by considering more subtle effects, e.g., determining on which side of the loop relative to the loop apex the largest amplitude displacement is located and comparing it with a simple model of the type considered here. However, it may be difficult to determine if the identified fundamental vertical mode is present together with the fundamental horizontal mode.

(2) The Doppler shift signatures provide additional constraints that can help distinguish between two types of kink modes which exhibit similar spatial oscillation signatures if the used spectrometers have a high resolution in Doppler velocity and if the spectrometer slit crosses the loop at two or more locations (or if the loop is scanned sufficiently rapidly) and if the studied loop is well isolated from the ambient loops.

(3) The re-examination of the swaying-like motions of the loop top observed in a 2D arcade loop simulated by Selwa et al. (2006) shows several features such as the period ratio and weak damping relative to the fundamental mode that are consistent with the theoretically expected ones for the vertical second harmonic oscillation. They could be evidence for the swaying-like motions resulting from the second-harmonic vertical mode in the loop. However, there are differences that suggest that the fundamental vertical mode was also excited. Simultaneous excitation of multiple modes complicates the identification further. The simple analysis presented here may not be adequate in such cases.

In Sect. 3.3 we only considered the shape of velocity profile along a loop, but the absolute amplitude of Doppler velocity may also be used to distinguish between different kink modes. The amplitude of Doppler velocity can be inferred from the apparent displacement amplitude divided by the measured oscillation period for a given geometry and oscillation mode. The amplitude is expected to be a strong function of the oscillation mode and could be used to identify the mode by comparing with direct measurements of Doppler velocity obtained with a slit spectrograph at only a single location.

We have determined which type of kink modes each of the 14 transverse loop oscillations observed by TRACE belongs to based on a comparison between the observed and modeled signatures (see the last two columns in Table 1). For 2 loops out of the 6 loops in Category I the oscillation corresponds to the fundamental vertical mode (but may be combined with the fundamental horizontal mode), and for another it is identified as the fundamental horizontal kink mode. The remaining 3 could not be uniquely identified. Out of the 6 loops in Category II one loop shows the interesting feature which first indicates the dominant vertical motion and then agrees with the combined fundamental vertical and horizontal modes. The oscillations of the other loops could not be uniquely identified. The two loops in Category III

are clearly identified as displaying the fundamental horizontal kink mode. The results suggest that horizontal oscillations seem to be more easily excited under solar condition. This may be because the disturbing sources (e.g., flares) are commonly located near to but rarely immediately in the plane of the oscillating loops. Note, however, that any vertical oscillations in loops of Category III would not easily have been detected in TRACE data.

In summary, our analysis has shown that for a given viewing geometry it may be difficult to distinguish between some of the different kink modes and in future when identifying kink modes the results of this work should be taken into account, and comparisons should be made to simple geometrical models, like those considered here. Ideally, the application of this method requires the complete loop to be well visible. This is not always the case with observed oscillating loops, which are sometimes only partially visible.

The current analysis is not complete. Thus, it is restricted to loops lying in a plane and does not consider the case of sheared loops such as that reported by De Moortel & Brady (2007). We have also not taken into account the information in the oscillation period, although it is affected by different atmospheric parameters and may not always help distinguish between modes. Another way of distinguishing between vertical and horizontal modes may be through brightness fluctuations (Wang & Solanki 2004), but before doing that improved statistics of vertical oscillations are needed. Finally, stereoscopy, when corresponding data are available, should be very helpful for obtaining the true geometry of oscillating loops and of the oscillations they harbor (e.g. Feng et al. 2007).

References

Andries, J., Arregui, I., & Goossens, M. 2005, ApJ, 624, L57
Aschwanden, M. J. 2004, Physics of the Solar Corona – An Introduction (Chichester UK: Praxis Publishing Ltd, and Berlin: Springer), 283
Aschwanden, M. J., Newmark, J. S., Delaboudiniére, J.-P., et al. 1999, ApJ, 515, 842
Aschwanden, M. J., Pontieu, B. D., Schrijver, C. J., & Title, A. 2002, Sol. Phys., 206, 99
Berghmans, D., & Clette, F. 1999, Sol. Phys., 186, 207
Brady, C. S., & Arber, T. D. 2005, A&A, 438, 733
Brady, C. S., Verwichte, E., & Arber, T. D. 2006, A&A, 449, 389
De Moortel, I., & Brady, C. S. 2007, ApJ, 664, 1210
De Moortel, I., Ireland, J., & Walsh, R. W. 2000, A&A, 355, L23
De Moortel, I., Ireland, J., Hood, A. W., & Walsh, R. W. 2002a, A&A, 387, L13
De Moortel, I., Hood, A. W., Ireland, J., & Walsh, R. W. 2002b, Sol. Phys., 209, 89
Díaz, A. J. 2006, A&A, 456, 737
Díaz, A. J., Zaqarashvili, T., & Roberts, B. 2006, A&A, 455, 709
Edwin, P. M., & Roberts, B. 1982, Sol. Phys., 76, 239
Edwin, P. M., & Roberts, B. 1983, Sol. Phys., 88, 179
Feng, L., Inhester, B., Solanki, S. K., et al. 2007, ApJ, 671, L205
McEwan, M. P., Donnelly, G. R., Díaz, A. J., & Roberts, B. 2006, A&A, 460, 893
McLaughlin, J. A., & Ofman, L. 2008, ApJ, 682, 1338
Miyagoshi, T., Yokoyama, T., & Shimojo, M. 2004, PASJ, 56, 207

Nakariakov, V. M. 2003, Dynamic Sun, ed. B. N. Dwivedi (Cambridge, UK: Cambridge University Press), 314

Nakariakov, V. M., & Ofman, L. 2001, A&A, 372, L53

Nakariakov, V. M., & Verwichte, E. 2005, Living Reviews in Solar Physics, 2, 3, http://www.livingreviews.org/lrsp-2005-3

Nakariakov, V. M., Ofman, L., DeLuca, E. E., et al. 1999, Science, 285, 862

Nakariakov, V. M., Verwichte, E., Berghmans, D., & Robbrecht, E. 2000, A&A, 362, 1151

Ofman, L., & Wang, T. J. 2002, ApJ, 580, L85

Roberts, B., & Nakariakov, V. M. 2003, NATO Advanced Workshop: Turbulence, Waves and Instabilities, ed. R. Erdélyi et al. (Kluwer Academic Publishers), 167

Roberts, B., Edwin, P. M., & Benz, A. O. 1984, ApJ, 279, 857

Schrijver, C. J., Aschwanden, M. J., & Title, A. M. 2002, Sol. Phys., 206, 69

Selwa, M., Murawski, K., Solanki, S. K., Wang, T. J., & Tóth, G. 2005, A&A, 440, 385

Selwa, M., Solanki, S. K., Murawski, K., Wang, T. J., & Shumlak, U. 2006, A&A, 454, 653

Selwa, M., Murawski, K., Solanki, S. K., & Wang, T. J. 2007, ApJ, 462, 1127

Terradas, J., Oliver, R., & Ballester, J. L. 2006, ApJ, 650, 91

Terradas, J., Andries, J., & Goossens, M. 2007, A&A, 469, 1135

Van Doorsselaere, T., Debosscher, A., Andries, J., & Poedts, S. 2004, A&A, 424, 1065

Van Doorsselaere, T., Nakariakov, V. M., & Verwichte, E. 2007, A&A, 473, 959

Verwichte, E., Nakariakov, V. M., Ofman, L., & Deluca, E. E. 2004, Sol. Phys., 223, 77

Verwichte, E., Foullon, C., & Nakariakov, V. M. 2006a, A&A, 446, 1139

Verwichte, E., Foullon, C., & Nakariakov, V. M. 2006b, A&A, 449, 769

Wang, T. J. 2004, in Proc. of SOHO 13, Waves, Oscillations and Small-Scale Transient Events in the Solar Atmosphere: A Joint View from SOHO and TRACE, ed. H. Lacoste, ESA SP-547, 417

Wang, T. J. 2005, in Proc. of the International Scientific Conference on Chromospheric and Coronal Magnetic Fields, ed. D. E. Innes, A. Lagg, S. K. Solanki, & D. Danesy, ESA SP-596, 42

Wang, T. J., & Solanki, S. K. 2004, A&A, 421, L33

Wang, T. J., Solanki, S. K., Curdt, W., et al. 2002, ApJ, 574, L101

Wang, T. J., Solanki, S. K., Innes, D. E., et al. 2003a, A&A, 402, L17

Wang, T. J., Solanki, S. K., Curdt, W., et al. 2003b, A&A, 406, 1105

Wang, T. J., Solanki, S. K., Innes, D. E., & Curdt, W. 2005, A&A, 435, 753

Wang, T. J., Innes, D. E., & Solanki, S. K. 2006, A&A, 455, 1105

Wang, T. J., Innes, D. E., & Qiu, J. 2007, ApJ, 656, 598